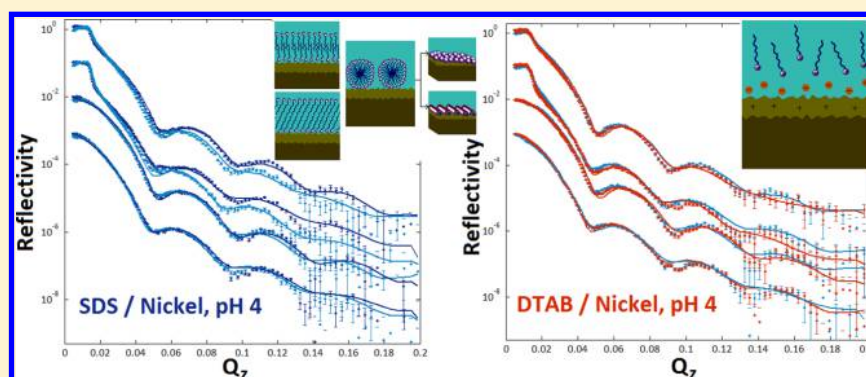


Polarized Neutron Reflectometry of Nickel Corrosion Inhibitors

Mary. H. Wood,[†] Rebecca J. L. Welbourn,[†] Ali Zarbakhsh,[‡] Philipp Gutfreund,[§] and Stuart M. Clarke^{*†}[†]Department of Chemistry and BP Institute, Cambridge University, Cambridge CB2 1EW, U.K.[‡]School of Biological and Chemical Science, Queen Mary, University of London, Joseph Priestly Building, Mile End Road, London, U.K.[§]Institut Laue-Langevin, Grenoble, France Supporting Information

ABSTRACT: Polarized neutron reflectometry has been used to investigate the detailed adsorption behavior and corrosion inhibition mechanism of two surfactants on a nickel surface under acidic conditions. Both the corrosion of the nickel surface and the structure of the adsorbed surfactant layer could be monitored in situ by the use of different solvent contrasts. Layer thicknesses and roughnesses were evaluated over a range of pH values, showing distinctly the superior corrosion inhibition of one negatively charged surfactant (sodium dodecyl sulfate) compared to a positively charged example (dodecyl trimethylammonium bromide) due to its stronger binding interaction with the surface. It was found that adequate corrosion inhibition occurs at significantly less than full surface coverage.

INTRODUCTION

Nickel is generally renowned for its high resistance to corrosion under ambient conditions due to the formation of a passive nickel oxide layer that is consequently slow to react with further oxidants^{1,2} and is therefore often used as a protective coating for other, more reactive, metals.³ It has been reported that the outermost protective layer formed on nickel in an aqueous environment is actually a nickel hydroxide, Ni(OH)₂, with an intermediate NiO layer.^{2,4}

However, when exposed to oxidizing acidic solutions, this resistance to corrosion is vastly reduced, and defects such as pitting develop.⁵ As nickel has many industrial uses that require exposure to an acidic environment,⁶ numerous additives have been proposed to protect the surface from these effects.^{1,7–16} These inhibitors are purported to form a physisorbed protective layer on the surface, ensuring that the metal is less prone to attack by corrosive species in solution^{14,17} in addition to polarizing the metal surface such that the potential difference between the anodic and cathodic areas is reduced.^{18–20}

In this work, the efficacy of two different surfactants, sodium dodecyl sulfate (hereafter SDS) and dodecyltrimethylammonium bromide (hereafter DTAB), as corrosion inhibitors for a nickel surface (modeled by the deposition of a 100 Å nickel film

on a silicon substrate) under acidic conditions was investigated using polarized neutron reflectometry (PNR). This was supported by ζ -potential data for characterizing changes in surface charge, X-ray photoelectron spectroscopy (XPS) for surface composition and oxidation states, X-ray reflectivity (XRR) to measure the metal film thickness, and depletion isotherms to determine the amounts of inhibitor adsorbed. The two additives were selected as representative paradigms of anionic (SDS) and cationic (DTAB) surfactants, as well as being very commonly used materials commercially; both are cited as having some success as corrosion inhibitors for nickel in acidic solutions.^{12,15,21}

Neutron reflectometry has previously been used for detailed investigation of corrosion mechanisms as it uniquely provides angstrom-level quantification of metal and oxide film growth or dissolution and film roughnesses.²² Wiesler et al. report the use of neutron reflectometry to monitor the corrosion of titanium films deposited on a silicon substrate in a 0.1 N H₂SO₄ solution.²³ Neutron reflectivity profiles were recorded for a series of

Received: May 9, 2015

Revised: June 4, 2015

Published: June 7, 2015

increasing applied potentials and were interpreted to show increased oxide layer thickness and decreased metal layer thickness with increased voltage. A simultaneous increase in surface roughness and hydrogen ingress into the layer was also reported. Similarly, Barkhudarov et al. have used neutron reflectometry to prove the adequacy of superhydrophobic films to protect aluminum surfaces from corrosion.²⁴

We have previously demonstrated the use of PNR for the study of adsorption on a magnetic iron film,^{25,26} as neutrons with their spin aligned parallel and antiparallel with the layer magnetization (hereafter referred to as “up-spin” and “down-spin”) interact differently with the sample, the collection of neutron reflectivity profiles for the two different polarizations yields an additional contrast, which further constrains the model-fitting process and improves the likelihood of finding the unique structural solution. This is particularly useful for corrosion studies, where the two spin-state data sets are obtained simultaneously rather than sequentially. As changes in the surface structure may occur between solvent exchanges, this approach uniquely permits the collection of two contrasts for each stage in the corrosion process.

The ability to contrast match in neutron reflectometry makes it a particularly powerful surface-study tool;^{27,28} the scattering length densities (SLDs) of deuterated and protonated solvents are significantly different, such that a careful choice of the mixture of the two permits the selection of an SLD to match that of other layers in the system. Changes in data may then be attributed as arising mainly from non-contrast-matched components, so the model may be greatly simplified. The use of contrast matching is particularly apt for the nickel/surfactant systems of interest here. SLD values for the materials used in this study are shown in Table 1. Although the SLD of nickel for

Table 1. SLD Values

	$\rho / \times 10^{-6} \text{ \AA}^{-2}$		$\rho / \times 10^{-6} \text{ \AA}^{-2}$
Si	2.072	SiO ₂	3.480
Ni (up spin)	10.86	Ni (down spin)	7.940
NiO	8.661	Ni(OH) ₂	3.843
H ₂ O	-0.561	D ₂ O	6.335
SDS	0.337	DTAB	-0.220

both up- and down-spin neutrons is higher than that of even pure D₂O such that the solvent cannot be completely matched to the nickel surface, by characterizing the system consecutively under D₂O and H₂O the emphasis may be shifted almost entirely from the surfactant layer structure to the metal surface, as shown by the SLD profiles in Figure 1. This enables separate characterization of the adsorbed layer and corroding metal surface.

EXPERIMENTAL SECTION

Materials. Substrates for neutron experiments were prepared by sputtering nickel films to a thickness of approximately 100 Å onto a polished silicon substrate, (111) orientation, (n) type, of diameter 55 mm and thickness 5 mm, using reactive magnetron sputtering in vacuo²⁹ at the Nanoscience Centre at the University of Cambridge. For XPS and XRR measurements the same method was used on smaller substrates (10 × 10 × 0.5 mm³). Nickel oxide (NiO) powder used in ζ -potential and isotherm measurements was purchased from Fuel Cell Materials, with a BET surface area of 3.7 m² g⁻¹ (as determined by the adsorption of nitrogen at the Department of Chemical Engineering and Biotechnology, University of Cambridge). Other chemicals were purchased from Sigma-Aldrich and used without

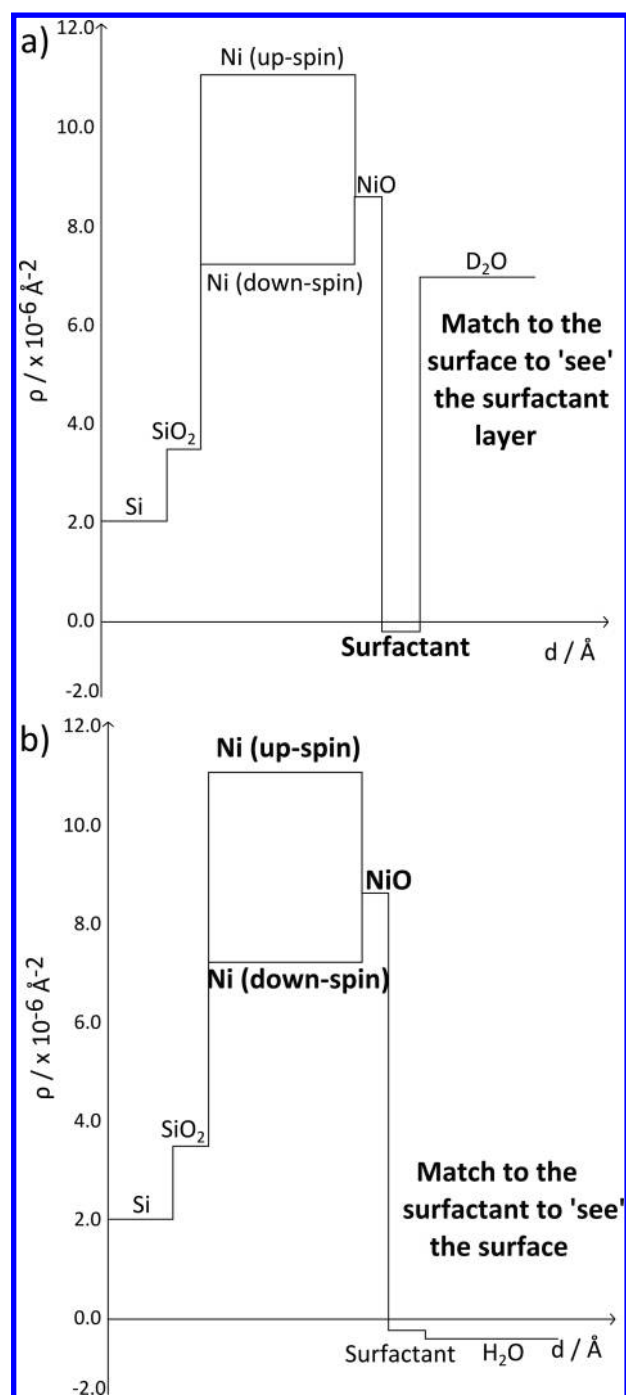


Figure 1. By using (a) D₂O or (b) H₂O as the bulk solvent, the surfactant layer or metal surface may be selectively emphasized as shown.

further purification (all had purities >99% as determined by GC and titration). The purities of SDS and DTAB were confirmed using surface tension measurements, which showed no evidence of a dip at the critical micelle concentration (CMC), which would be indicative of surface-active impurities.

XPS. XPS measurements were taken at the NEXUS laboratory (Newcastle University, U.K.) using the AXIS Nova XPS spectrometer. XPS spectra were recorded for the films as-sputtered and also for those cleaned using UV/ozone (30 min). Spectra were fitted using the CasaXPS software and calibrated by setting the C 1s peak to 285.0 eV.

XRR. XRR measurements were carried out at the Cavendish Laboratories in Cambridge using a Bruker D8 X-ray diffractometer with a copper target and a Goebel mirror. An accelerating voltage of 40 kV

and a primary beam size of 0.1 mm were used. The detector was operated in single pixel (0D) mode. Samples were cleaned with UV/ozone (30 min) before being soaked in ultrapure water (UPW) adjusted to the required pH by the requisite volume of nitric acid for 2 h and dried using a flow of N_2 gas before measurement. Data were fitted to a structural model using GenX 2.0 software to minimize the figure of merit (FOM).³⁰ The Parratt algorithm was used to generate the model fits.³¹

ζ Potential. To measure the ζ potential of the NiO powder over a range of pH values, solutions of sodium nitrate (concentrations 1–100 mM) were adjusted to each pH as required using nitric acid or sodium hydroxide. NiO powder (1 mg mL^{-1}) was then dispersed in the solution, and the average particle size and ζ potential were measured using a Brookhaven ZetaPALS dynamic light scatterer. Further profiles were measured at 10 mM sodium nitrate concentration, with the addition of either 7 mM SDS or DTAB to the dispersion.

Solution Depletion Isotherms. Solution depletion isotherms of SDS and DTAB on the NiO powder were obtained in sodium nitrate-buffered (0.01 M) aqueous solution at pH 2 and 4. Samples (over a concentration range of 0–20 mM) were tumbled with NiO powder (1 g) over a period of 24 h to ensure that equilibration was attained. The solid was then separated by centrifugation, and the final concentration of the supernatant in each case was measured using a total organic carbon analyzer (Sievers InnovOx 3.00).

PNR. PNR measurements were collected using the D17 instrument at the Institut Laue-Langevin in Grenoble, France. The instrument was run in monochromatic, polarized mode, with vertically mounted samples and a vertical guidefield at the sample position between 250 and 300 G. The neutron wavelength used was 5.6 \AA with a resolution of $\Delta\lambda/\lambda = 6\%$ (fwhm). The polarization of the incoming beam was $98.7 \pm 0.05\%$, and the efficiency of the spin flipper was $97 \pm 0.3\%$. The measurements were performed by measuring the reflectivity of the two aforementioned spin states without polarization analysis. The beam footprint on the sample was fixed to $(35 \times 35) \text{ mm}^2$, and the angular divergence of the incoming beam was $\Delta\theta/\theta = 3\%$ (fwhm).

Two nickel-sputtered silicon substrates (hereafter referred to as substrates 1 and 2 for convenience) were cleaned using UV/ozone (30 min) before being enclosed in custom-designed cells, as successfully used previously.²⁶ These were passed through a magnetic field of 1000 G next to the parallel guidefield in order to saturate the Ni magnetization before being secured in the beam path without leaving the guidefield at any point. Both substrates were characterized under pure H_2O and pure D_2O in order to extract the nickel film and oxide layer thicknesses and roughnesses. To substrate 1, a 5 mM solution of SDS at pH 6 was then added, and the surfactant layer was characterized under both water contrasts. Solutions (5 mM) at pH 4 and 2 were consecutively flushed through the sample cell, and neutron reflectivity profiles were obtained at each pH for both water contrasts. The same approach was adopted for substrate 2, using 5 mM DTAB as the additive rather than SDS. The concentration value of 5 mM, lying below the CMC of both SDS and DTAB over the whole pH range of interest here, was chosen from the depletion isotherm data as a concentration at which significant SDS adsorption was known to occur. The PNR data were fitted to a structural model using the Rascal fitting program to minimize χ^2 . Calculations indicated that the small element of beam depolarization (approximately 3%), combined with the similarity of the given Ni spin up- and down-spin SLDs, did not lead to a significant difference in the structural characterization of the layers and hence the data sets were fitted as pure up-spin and down-spin systems.

RESULTS AND DISCUSSION

XPS. Comparison of the XPS survey spectra for nickel films cleaned using a range of different methods demonstrated that exposure to UV/ozone for 30 min was most effective at reducing the C 1s peak and thus removing surface contamination. This process was consequently adopted as the standard cleaning procedure in this work. Representative spectra for the Ni 2p region are shown in Figure 2, comparing an untreated film (i)

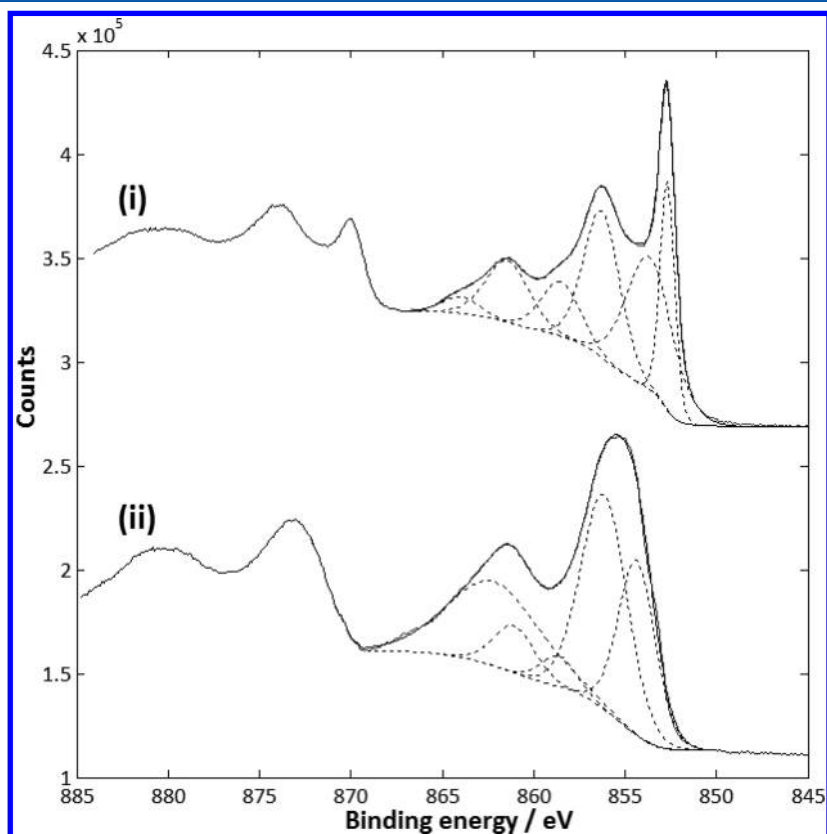


Figure 2. Ni 2p region for (i) the precleaned film (normalized to higher counts for ease of viewing) and (ii) the cleaned film. Data are shown in gray, with the fit shown in black and individual fitted peaks as dotted lines.

with one cleaned by UV/ozone (ii). The oxidizing nature of the cleaning process has clearly significantly changed the surface composition; the untreated film shows some Ni metal present; this is entirely lost in the cleaned film, which entirely comprises a mixture of oxide and hydroxide. While the fitting of XPS spectra is a nontrivial matter and is not attempted in detail here, reasonable fits for the $2p_{3/2}$ regions of both spectra are shown in Figure 2, with the peak assignments summarized in Table 2.

Table 2. XPS Peak Fits for the Nickel Film $2p_{3/2}$ Regions

assignment	binding energy/eV	area %	fwhm/eV
Nickel Film Precleaning			
Ni $2p_{3/2}$	852.48	16.66	1.0
NiO $2p_{3/2}$	853.45	30.42	3.0
Ni(OH) $_2$ $2p_{3/2}$	856.07	26.29	2.3
NiO $2p_{3/2}$ satellite	858.31	10.44	2.5
Ni(OH) $_2$ $2p_{3/2}$ satellite	861.23	13.22	2.8
shake-up structure	863.79	2.97	2.3
Nickel Film after UV/Ozone Cleaning			
NiO $2p_{3/2}$	854.35	23.90	2.4
Ni(OH) $_2$ $2p_{3/2}$	856.15	36.44	3.0
NiO $2p_{3/2}$ satellite	858.63	3.96	2.3
Ni(OH) $_2$ $2p_{3/2}$ satellite	861.06	7.15	2.6
shake-up structure	862.16	28.55	5.9

The least number of peaks possible was used to obtain a plausible fit, which shows the presence of Ni metal in the untreated film along with the two main species—the oxide NiO and hydroxide Ni(OH) $_2$ —with their respective satellite peaks at slightly higher binding energies. The oxide and hydroxide are seen exclusively in the cleaned film. The fit also necessitated the inclusion of a broad peak at 862.16 eV; this is attributed to a “shake-up” structure (caused by the interaction of the ejected

photoelectron with the ion it is leaving, resulting in its further excitation, and overall decreased energy of the photoelectron to produce a peak at an apparent higher binding energy) and other intrinsic losses, as observed by several other authors for Ni 2p spectra.^{32–34}

XRR. The X-ray reflection (XRR) data for a sample cleaned by UV/ozone is shown in Figure 3(i). The best fit an oxide layer that was resolved into two equal layers with densities corresponding to those expected for NiO and Ni(OH) $_2$, in good agreement with the XPS data. The nickel film was subsequently soaked in HNO $_3$ (0.1 M, pH 1.0) for 1 h, and the XRR profile was measured, as also shown in Figure 3(ii). It is clear that essentially the entire nickel layer has been dissolved, with a very thin, highly roughened layer remaining.

ζ Potential. The ζ -potential results are shown in Figure 4. Data were measured over a range of background salt concentrations (Figure 4a) to confirm that sodium nitrate acts as an indifferent electrolyte.³⁵ The increasing slope steepness for lower concentrations is attributed to the overall lower ionic strength; the potential will fall more quickly with distance from the surface.³⁶ From these data, the point of zero charge (PZC) for the NiO surface was determined to lie in the pH range of 6.7–7.4. This agrees well with literature values³⁷ (although variance is seen for differing conditions) and indicates a positively charged metal surface for the pH range studied here. Figure 4b also shows the ζ -potential curves for the surface in 0.01 M sodium nitrate with added surfactant. It is clear that upon addition of 7 mM DTAB the surface remains positively charged across the entire pH range measured, whereas the addition of 7 mM SDS renders the surface negatively charged across the range measured. These data clearly indicate significant adsorption of the SDS at acidic pH such that the positively charged surface is both neutralized and even rendered negative by SDS adsorption. In contrast, at these pH values, the

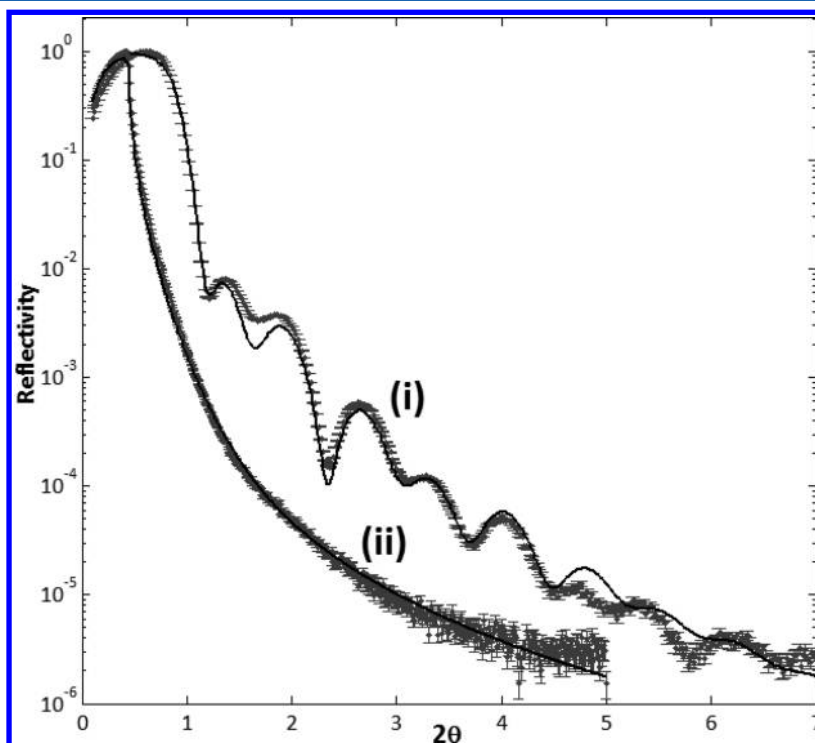


Figure 3. XRR data for the nickel film (i) in air and (ii) after exposure to HNO $_3$ (0.1 M) for 1 h with model fits shown as black lines.

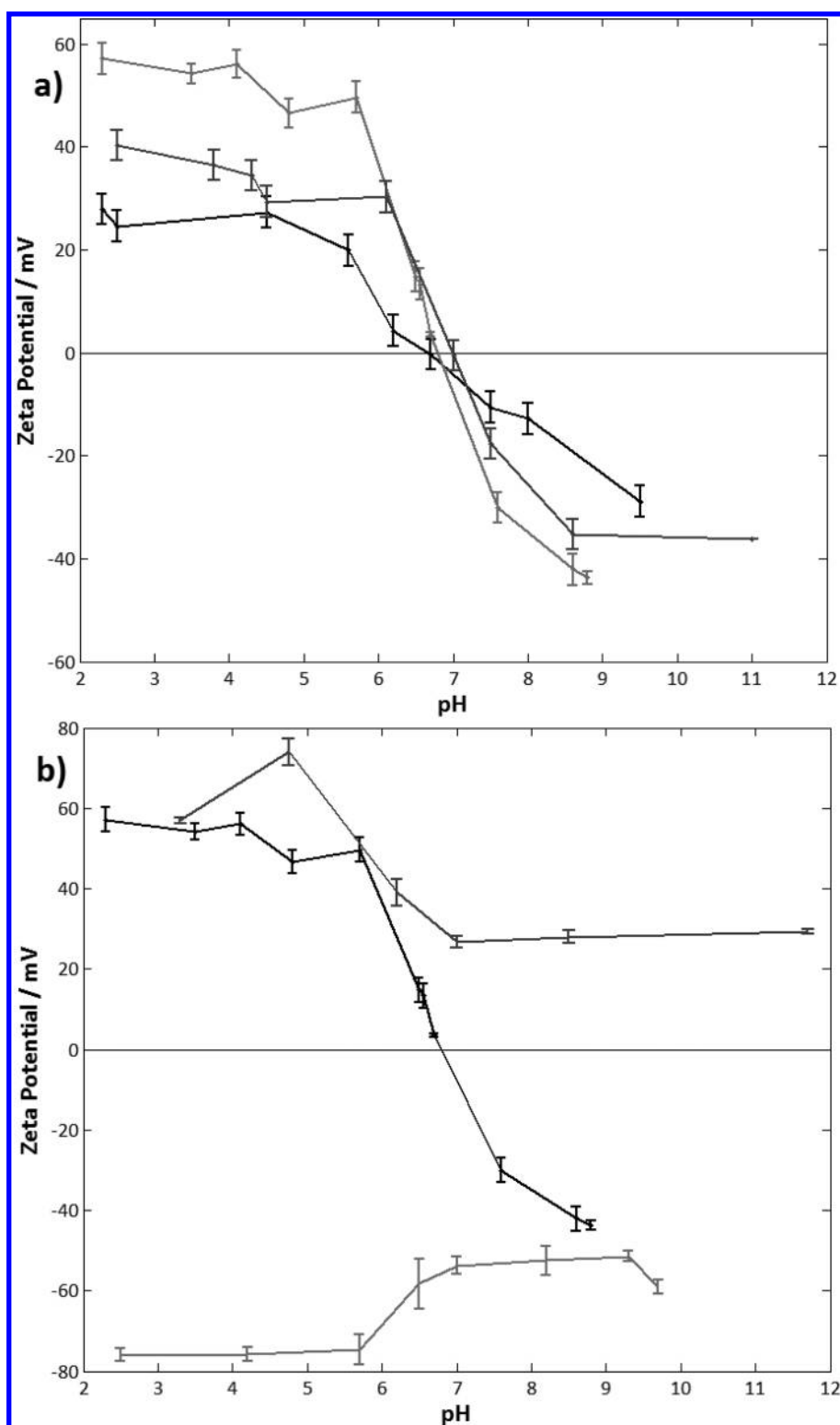


Figure 4. (a) ζ -potential curves for NiO powder in sodium nitrate solution over a range of concentrations (black, 0.1 M; dark gray, 0.05 M; light gray, 0.01 M). (b) ζ -potential curves for NiO powder in 0.01 M sodium nitrate solution (black) with added 7 mM DTAB (dark gray) or SDS (light gray).

DTAB has little effect on the surface charge, although it does keep the surface positively charged at higher pH.

Solution Depletion Isotherms. The depletion isotherms of SDS and DTAB on NiO powder in 0.01 M sodium nitrate solution are shown in Figure 5. It is immediately clear that SDS and DTAB exhibit very different behavior at the pH values

measured, with SDS showing far greater amounts adsorbed than positively charged DTAB. Using the linear regression method, isotherms were fitted to Langmuir, Freundlich, and BET isotherm models, with the latter showing the best fit to the data (as shown in Figure 5), signifying multilayer adsorption. This is also supported by the areas per molecule; for SDS the

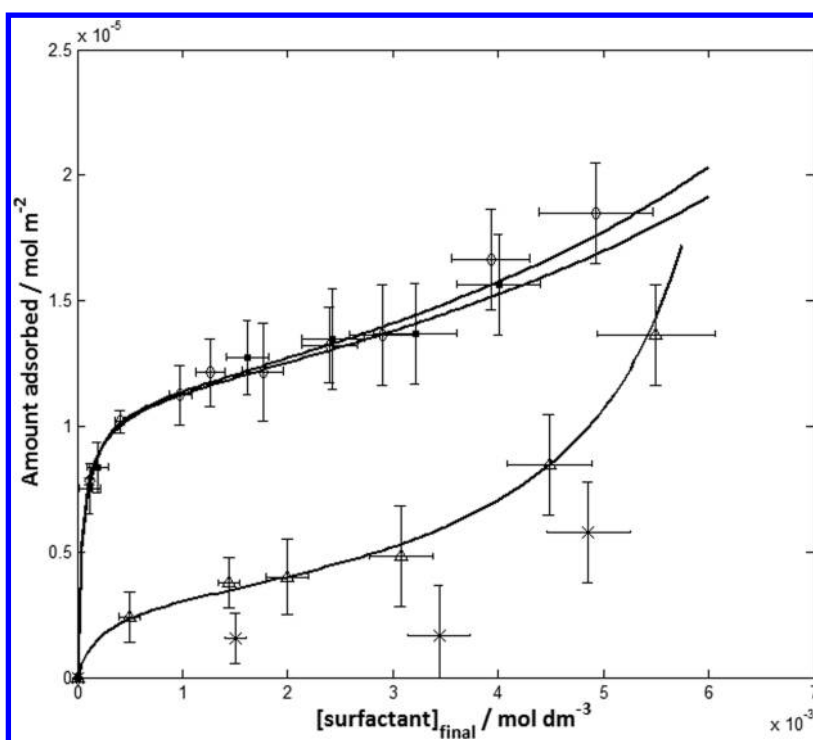


Figure 5. Isotherms of SDS (\diamond pH 4 and \bullet pH 2) and DTAB (Δ pH 4 and \times pH 2). BET models are shown as lines.

area per 2 molecules for an equilibrium concentration of 3 mM is 24 \AA^2 ($\pm 5 \text{ \AA}^2$); as the headgroup area is expected to occupy just under 20 \AA^2 ,³⁸ this would imply the formation of a bilayer. This is plausible; a monolayer would be unfavorable due to interactions of the hydrophobic tail with water, which are prevented by the formation of a bilayer. SDS seems to adsorb similarly at both pH 4 and 2, which is consistent with the plateau observed in the ζ -potential graph at low pH (Figure 4).

For DTAB, significantly less adsorption is seen, with an area per 2 molecules of 69 \AA^2 ($\pm 5 \text{ \AA}^2$) for pH 4 at an equilibrium concentration of 3 mM; at pH 2, barely any adsorption is seen within the experimental error. That there is any DTAB adsorbing at all at pH 4 is somewhat surprising, given the presumed repulsion between the positively charged surfactant and positively charged surface. Potential explanations are discussed in the PNR section below.

PNR. Neutron reflectivity profiles (plots of the measured reflectivity as a function of momentum transfer perpendicular to the surface) were initially collected for both nickel substrates 1 and 2 under D_2O and H_2O in order to characterize the nickel and oxide layers before adding surfactant. For substrate 1, a nickel film of thickness $116 (\pm 3) \text{ \AA}$ (agreeing well with the estimated deposition thickness) and roughness 5 \AA and a NiO film of thickness $23 (\pm 2) \text{ \AA}$ and roughness 7 \AA were modeled. Similar parameters were observed for substrate 2, with a nickel film of $123 (\pm 3) \text{ \AA}$ thickness and 5 \AA roughness and a NiO thickness of $19 (\pm 2) \text{ \AA}$ with roughness 7 \AA . While the XPS data clearly show a mixture of nickel hydroxide, $\text{Ni}(\text{OH})_2$, and oxide, NiO, at the surface, the hydroxide is harder to see in the PNR data; the best fit is obtained with an oxide of high density (i.e., NiO with no H present, as H has a low SLD). This is attributed to the exchange of surface H with H or D in the solvent. The addition of a hydroxide layer (either $\text{Ni}(\text{OD})_2$ or $\text{Ni}(\text{OH})_2$, depending on the contrast) to the model calculations did nothing to enhance the fit and so was not included.

For substrate 1, upon addition of a 5 mM solution of SDS, a surfactant layer is clearly seen to form at the surface. The data for the bare metal surface are compared to those for the added SDS in Figure 6a. For the D_2O contrasts, where we would expect to see changes due to the surfactant layer (as demonstrated in Figure 1), a clear difference is seen, indicating significant SDS adsorption onto the nickel surface, as observed in the depletion isotherm. To determine the surfactant layer structural parameters, three different layer models were fitted to the data for comparison, shown schematically in Figure 7a–d. Initially, a simple block layer was fitted with a thickness of $29 (\pm 2) \text{ \AA}$ (hydration 40%, roughness 7 \AA). As the length of the extended molecule is known³⁹ to be around 18 \AA , this may imply an interdigitated or tilted bilayer (shown in Figure 7a,b) or simply the effect of chain folding and cis conformations rather than a rigid straight chain.

However, while the concentration of the SDS solution was well below the critical micelle concentration⁴⁰ (CMC) of 8 mM, it is possible that a high local surfactant concentration at the surface may lead to micelle formation, an adsorption model that has been postulated previously for SDS and other surfactants on various surfaces. (For example, Li et al. attribute neutron reflectometry data for SDS on alumina surfaces to an oblate micellar structure.⁴¹) As the fitted hydration of the bilayer was close to that which might be expected for a spherical volume on the surface, two custom layer models were tried that fitted either cylindrical or spherical micelles adsorbed at the surface (depicted schematically in Figure 7c,d). Details of the fitting process and the fits themselves may be found in the Supporting Information. However, there was no obvious improvement in the fit seen by using either of the micellar models, with similar χ^2 values for all three models tried. Specular neutron reflectometry gives structural information pertaining to the z plane and hence lacks sensitivity to in-plane structure. Therefore, it is not possible to determine which of these three

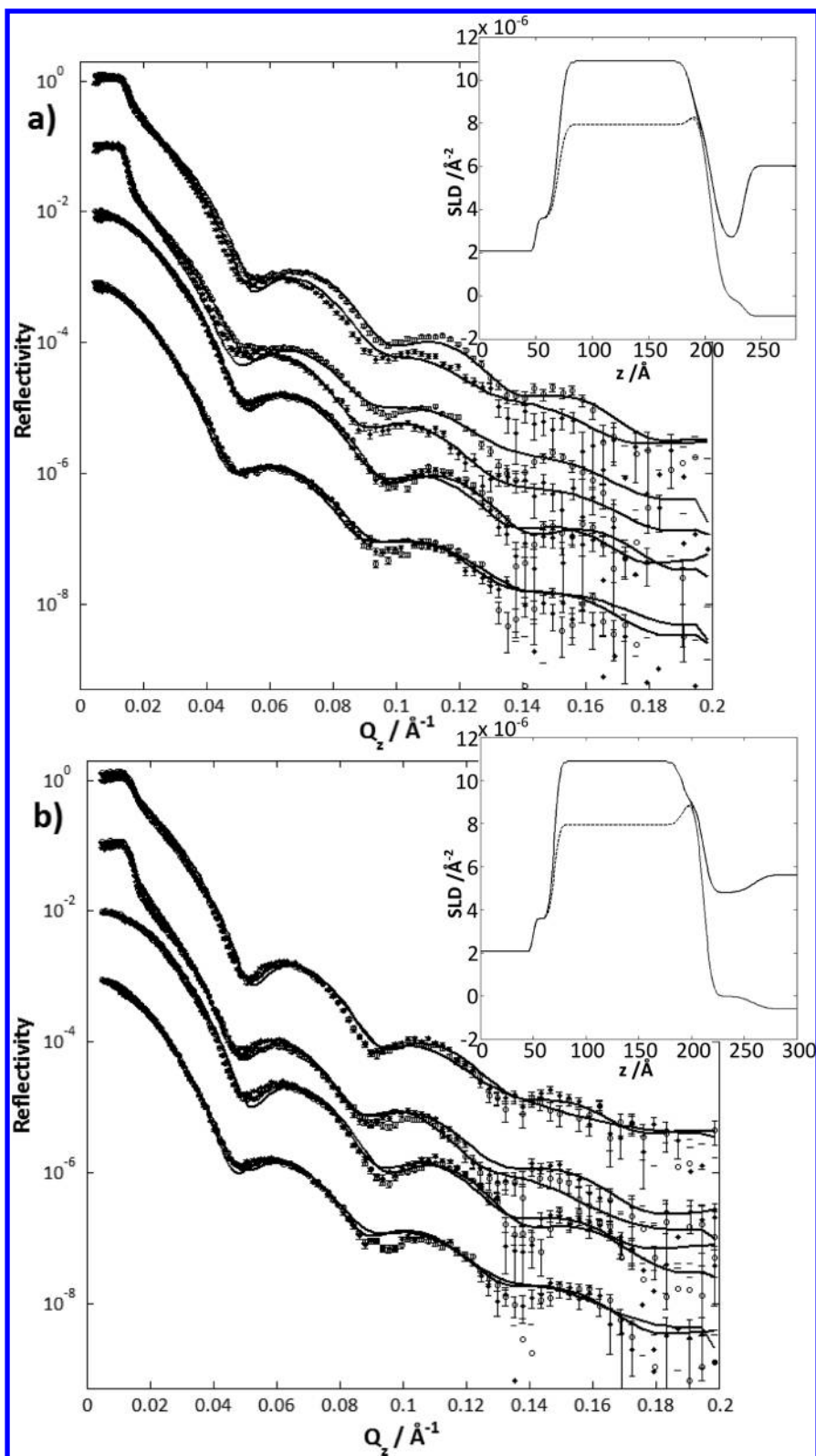


Figure 6. PNR data for (a) substrate 1 and (b) substrate 2, for the bare substrate under water (\bullet) and upon addition of 5 mM SDS (a) or DTAB (b) at pH 4 (\circ). In each case data are shown in descending order: up-spin D_2O , down-spin D_2O , up-spin H_2O , and down-spin H_2O . (Subsequent profiles are divided by 10 for the purpose of clarity.) Solid lines show model fits to the data. Insets show the fitted SLD profiles for the surfaces plus surfactant layers at pH 4.

models best describes the SDS system without further structural studies, although the lack of any significant increase in the background upon addition of SDS may support a more ordered bilayer rather than the micellar structures proposed.

The SDS layer thicknesses for all three models were very similar at 27–29 Å. Using the fitted thickness values and the % coverage value (taken to be the hydration value for the bilayer or the fractional volume of a cylinder or sphere respectively) to

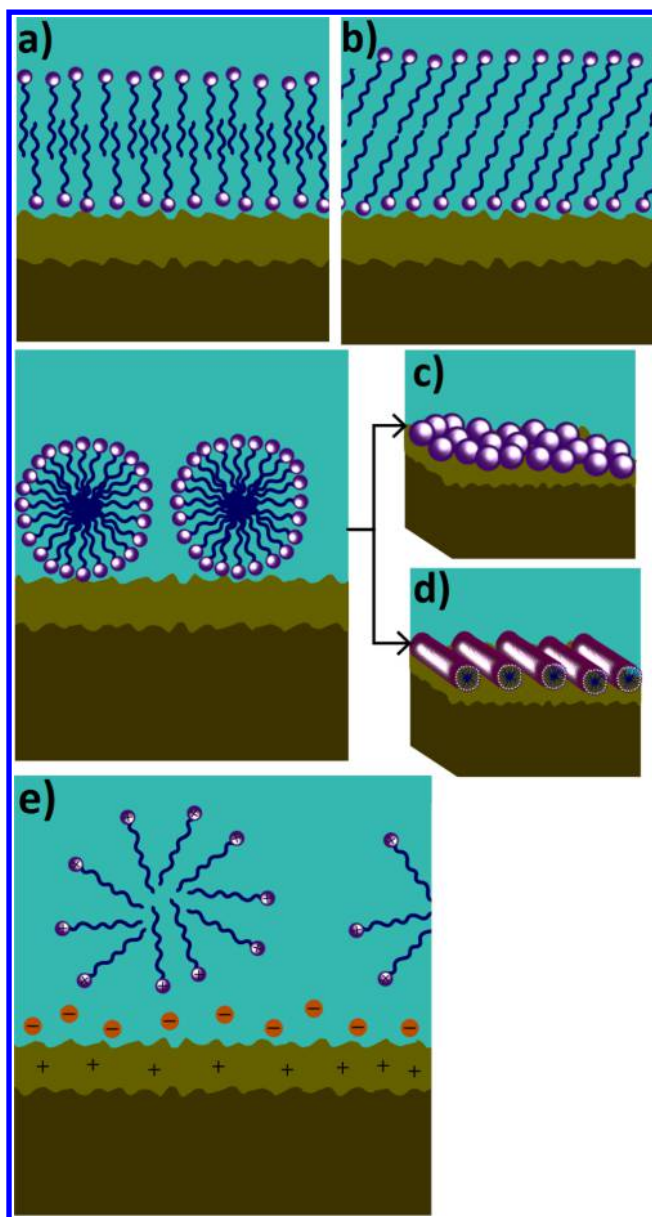


Figure 7. Schematics of fitted models for (a–d) SDS and (e) DTAB. (a) Interdigitated bilayer, (b) tilted bilayer, (c) spherical micelles, (d) cylindrical micelles, and (e) anion-mediated adsorption.

calculate the surface coverage (assuming molecular volumes of $4.741 \times 10^{-28} \text{ m}^3$ and $2.996 \times 10^{-29} \text{ m}^3$ for SDS and D_2O , respectively, calculated from their literature densities and molecular weights), coverage values of between 1.72×10^{-5} and $1.85 \times 10^{-5} \text{ mol m}^{-2}$ were obtained for pH 4. As can be seen from Figure 5, the higher limit of this range is slightly greater than the value expected from the depletion isotherms, but as the back calculation from the PNR data assumes an unrealistically entirely flat, smooth surface, it is not unreasonable that it overestimates the coverage value (since within each “flat” square meter the surface area is actually larger due to roughness), so this is taken to be satisfactory agreement between the two methods. While the two methods do present slightly different systems in that a powdered surface may not always interact with components in solution in the same way as a planar surface, it is clear that in this case the two techniques give rise to the same conclusions. For these experiments, the

powder used was of sufficiently large particle size that it may be considered to be an adequate model for the planar surface.

For substrate 1, when the pH was lowered to 2, very little change was observed in the metal film structure (shown by the similarity of the H_2O contrast data in Figure 8a) even for

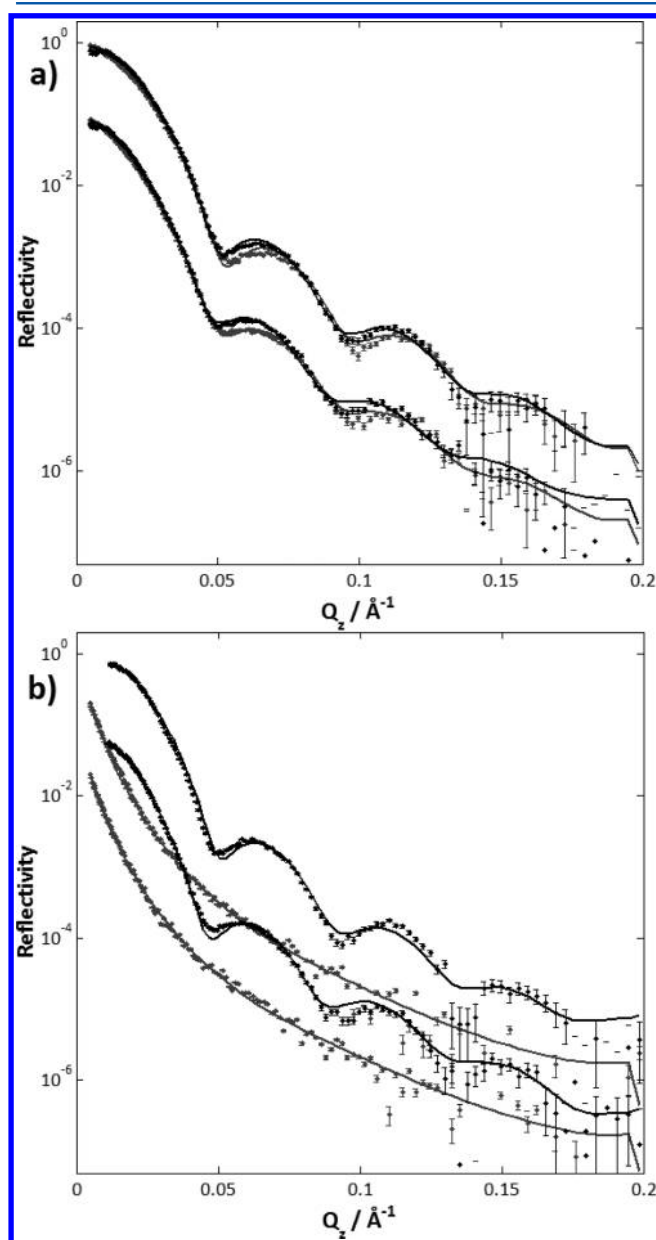


Figure 8. H_2O data (points) and fits (lines) at pH 6 (black) and pH 2 (gray) for (a) SDS data and (b) DTAB data.

measurements taken after 12 h; the nickel thickness had not changed within the error margins of the model, as it was found to have “decreased” to $114 (\pm 3) \text{ \AA}$, with a small increase in the NiO film thickness of 4 \AA . The Ni film roughness had also increased to 12 \AA , indicating that some corrosion had occurred. However, as the loss of 2 \AA Ni over 12 h equates to only 0.146 \mu m per year, corrosion may be said to occur at a negligible rate. Little change in the SDS thickness was observed for any model, although a slight increase in roughness was seen. This agrees well with the depletion isotherm data.

For substrate 2, when 5 mM DTAB was added, a small change was seen in the D_2O data (Figure 6b), signifying some

layer formation, though much less so than for SDS. However, the only plausible fit to the PNR data is obtained by fitting an interlayer of water (14 Å thick, roughness 3 Å) between the metal surface and a 33 (± 2) Å thick layer of DTAB, with a roughness of 10 Å and 61% hydration. When the pH is lowered to 4, the DTAB layer and interlayer thicknesses do not change within the error margins, but the DTAB hydration increases to 74%, indicating a highly disperse layer. Clearly, DTAB shows much less affinity for the surface, as would be expected from the DTAB and ζ -potential data.

As noted above, the adsorption of DTAB is surprising given that both the surfactant and nickel surface are positively charged at these pH values. Yet this is observed in both depletion isotherm and PNR data. One possible explanation for this behavior is a model of anion-mediated adsorption by means of the bromide anion (depicted schematically in Figure 7e). It is assumed from both the isotherm and PNR data that this would take the form of disperse, elongated micelles rather than an energetically unfavorable monolayer. While the phenomenon of cation bridging is well documented in the literature,^{42,43} there is scant reference to the possibility of an anionic equivalent. However, anions have long been recognized as providing “bridges” between oxidized metal centers as ligands in electron-transfer mechanisms in solution,⁴⁴ so it is reasonable to suggest that given the right conditions they could provide a similar function at the surfactant–metal surface interface. Anionic polymers are known to provide bridges between positively charged amine layers to promote their adsorption.⁴⁵ Ma et al. account for adsorption of cetyltrimethylammonium bromide (CTAB) on copper surfaces via a similar anion-bridging mechanism,^{46,47} and Rudnik et al. observe the adsorption of CTAB onto positively charged SiC surfaces, although they attribute this to patches of negative or neutral charge on a surface with overall positive charge.⁴⁸ More significantly, there exist several studies on the corrosion of iron in acidic solutions where it has been suggested that the preadsorption of halide ions to the positively charged iron surface can promote the adsorption of positively charged surfactants with ammonium headgroups and thus hinder corrosion synergistically. In these studies the effect is most enhanced for the iodide anion, I⁻, but may also be seen for bromide ions.^{49–53} Significant cation bridging has been observed previously only for multivalent cations, presumably due to their need to simultaneously bind both to anionic surface groups and the anionic surfactant, although Franchi et al. observe some effect of cation bridging for nucleic acids on positively charged clay surfaces at high sodium ion concentrations.⁵⁴ Bromide ions are known to adsorb to metal surfaces and are indeed sometimes thought to contribute to their corrosion;^{55,56} therefore, it is conceivable that the Br⁻ ions from the DTAB molecules are interacting with the nickel surface so that the remaining DTA⁺ ions are weakly attracted to the interface.

Neutron reflectometry studies concerning cation bridge-mediated adsorption do not document the hydrated interlayer seen here.⁴² While the Ca²⁺ ion is considerably smaller than the Br⁻ ion due to electron repulsion in the latter, this size difference is probably not great enough to account for the fitted water layer thickness; however, when taking into account the hydration value of 6 for the bromide ion⁵⁷ as well as possible bound water molecules on the nickel oxide surface and given that the bromide ion and water molecule have radii of approximately 2 and 1.5 Å, respectively, in aqueous solution,⁵⁸ an overall thickness of around 14 Å for the water interlayer is

certainly not unreasonable. The greater surface–surfactant distance may also be attributed to the weakness of the interaction in this instance, as Br⁻ is a so-called “soft” anion.

When a 5 mM DTAB solution at pH 2 was flushed through the cell, the entire Ni layer was seen to dissolve in under 6 h, as clearly evident in the H₂O data (Figure 8b) with the fringe structure completely lost. The separation between the two data sets for up- and down-spin neutrons is also lost, signifying the lack of any net magnetization and hence the loss of magnetized material, i.e., nickel metal. In addition, the overall intensity has dropped, corresponding to an increase in roughness; a significant increase in off-specular scattering was also observed at this pH, corroborating the roughness increase observed by the specular signal.

While this work has focused mostly on the development of the techniques described for the nickel surfaces and hence two surfactants were chosen that were mainly comparable in structure with the exception of their headgroups, which have different charges and chemistry, it does perhaps raise some interesting questions about the nature of the ideal corrosion inhibitor. Although the action of a corrosion inhibitor has sometimes been described as purely providing a physical barrier between the surface and attacking species in solution, it is clear that a well-packed dense layer is not always necessary because in this case the SDS layer has a coverage of only around 60% and yet is still sufficient to prevent corrosion. It may, therefore, be presumed that the interaction between the adsorbate headgroup and surface is of paramount importance, and indeed it has been suggested that the primary action of corrosion inhibitors is to bind to specific active sites on the surface such that only a relatively low concentration of inhibitor, significantly below full surface coverage, is required to passivate it.^{59,60} A key role of the alkyl chain may lie, therefore, in facilitating the optimal solubility and transport kinetics of the inhibitor rather than simply acting as a physical barrier; a short-enough chain is needed to ensure a high-enough solubility for sufficient surfactant to reach the surface, but the solubility should not be too high such that upon binding the adsorbate does not then pull the metal ions away, thus corroding, rather than passivating, the surface.

CONCLUSIONS

All of the techniques used in this study have clearly shown that while DTAB is entirely ineffective at protecting nickel surfaces from the effects of corrosion in an acidic medium, SDS prevents significant corrosion (scaled to $<0.2 \mu\text{m year}^{-1}$) at pH 2, although some surface roughening is seen, indicating that it cannot be considered to be a perfect corrosion inhibitor. The method also highlights the extreme sensitivity of the PNR approach to even tiny levels of corrosion that would be completely invisible by other more traditional methods. A significant amount of adsorbed SDS is observed from both depletion isotherm and PNR data, although its exact structure on the surface remains uncertain, with spherical and cylindrical micellar structures possible; these cannot be distinguished in this instance from a tilted or interdigitated bilayer. The use of PNR is demonstrated as a useful tool to obtain detailed parameters for the corrosion inhibition mechanisms of surfactants on metals, due to the combination of contrast matching, to selectively monitor the surfactant or metal surface at any one time, with the ability to determine metal and oxide film thicknesses and roughnesses to angstrom-level accuracy. The PNR data for the DTAB system at pH 6 and 4, possibly

surprisingly, seemed to indicate some DTAB adsorption, albeit weak, with the existence of a hydrated interlayer. The origin of this layer is uncertain. An anion-mediated mechanism has been considered, whereby the Br⁻ anions interact simultaneously between the positively charged surface and surfactants. However, this weakly bound DTAB layer proved entirely ineffectual at protecting the surface from corrosion, with the complete dissolution of the nickel film observed within 6 h at pH 2.

■ ASSOCIATED CONTENT

■ Supporting Information

Details of mathematical expressions used to fit the two possible micellar models and comparisons of the model fits. The Supporting Information is available free of charge on the ACS Publications website at DOI: 10.1021/acs.langmuir.5b01718.

■ AUTHOR INFORMATION

Corresponding Author

*E-mail: stuart@bpi.cam.ac.uk.

Notes

The authors declare no competing financial interest.

■ ACKNOWLEDGMENTS

We thank Dr. Seung Yeon Lee, University of Cambridge, for BET powder surface area measurements. X-ray photoelectron spectra were obtained at the National Engineering and Physical Sciences Research Council (EPSRC) XPS User's Service (NEXUS) at Newcastle University, an EPSRC midrange facility. NR data were obtained on the D17 instrument, and samples were treated in the laboratories of the Partnership for Soft Condensed Matter (PSCM) at the Institut Laue-Langevin. M.H.W. is grateful for funding from the Oppenheimer Trust.

■ REFERENCES

- (1) Khaled, K. F. Enhancing behaviour of nickel in nitric acid and its corrosion inhibition using some thiosemicarbazone derivatives. *Electrochim. Acta* **2010**, *55*, 5375.
- (2) Smith, R. J.; Hummel, R. E.; Ambrose, J. R. The passivation of nickel in aqueous solutions - II. An *in situ* investigation of the passivation of nickel using optical and electrochemical techniques. *Corros. Sci.* **1987**, *27*, 815–826.
- (3) Liu, H.; Li, N.; Bi, S.; Li, D.; Zou, Z. Effect of organic additives on the corrosion resistance properties of electroless nickel deposits. *Thin Solid Films* **2008**, *516*, 1883.
- (4) Kitakatsu, N.; Maurice, V.; Hinnen, C.; Marcus, P. Surface hydroxylation and local structure of NiO thin films formed on Ni(111). *Surf. Sci.* **1998**, *407*, 36–58.
- (5) Friend, W. Z. *Corrosion of Nickel and Nickel-Base Alloys*; John Wiley & Sons: New York, 1980.
- (6) Beverskog, B.; Puigdomenech, I. Revised Pourbaix Diagrams for Nickel at 25–300°C. *Corros. Sci.* **1997**, *39*, 969–980.
- (7) Khadom, A. A.; Yaro, A. S.; Kadhum, A. A. H. Adsorption mechanism of some chemical amines inhibitors for corrosion inhibition of copper-nickel alloy in hydrochloric acid. *Corros. Sci.* **2009**, *12*, 1–16.
- (8) Aksüt, A. A.; Bilgiç, S. The effect of amino acids on the corrosion of nickel in H₂SO₄. *Corros. Sci.* **1992**, *33*, 379–387.
- (9) Abd El Aal, E. E.; Zakria, W.; Diab, A.; Abd El Haleem, S. M. Aniline and some of its derivatives as corrosion inhibitors for nickel in 1 M HCl solution. *J. Chem. Technol. Biotechnol.* **1999**, *74*, 1061–1068.
- (10) Chen, Y. C.; Kuo, S. L.; Lee, J. L.; Ke, S. T.; Wong, C. H.; Ger, M. Der. The influence of surfactant CTAB on the microstructure and material properties of nickel microelectroforming. *Key Eng. Mater.* **2008**, *364–366*, 346–350.
- (11) Abdallah, M.; El-Etre, A. Y. Corrosion inhibition of nickel in sulfuric acid using tween surfactants. *Port. Electrochim. Acta* **2003**, *21*, 315–326.
- (12) Lu, J.; Yang, Q.; Zhang, Z. Effects of additives on nickel electrowinning from sulfate system. *Trans. Nonferrous Met. Soc. China* **2010**, *20*, s97–s101.
- (13) Fouda, A. S.; Mostafa, H. A.; Ghazy, S. E.; Farah, S. A. E.-. Use of hydrazone derivatives as inhibitors for the corrosion of nickel in hydrochloric acid solution. *Int. J. Electrochem. Sci.* **2007**, *2*, 182–194.
- (14) Hamed, E.; Abd El-Rehim, S. S.; El-Shahat, M. F.; Shaltot, A. M. Corrosion inhibition of nickel in H₂SO₄ solution by alanine. *Mater. Sci. Eng., B* **2012**, *177*, 441–448.
- (15) Guo, R.; Liu, T.; Wei, X. Effects of SDS and some alcohols on the inhibition efficiency of corrosion for nickel. *Colloids Surf., A* **2002**, *209*, 37–45.
- (16) Bholra, S. M.; Chandra, C.; Singh, G. Studies on the inhibition of nickel corrosion in dilute nitric acid by thiamine hydrochloride. *Corros. Sci.* **2008**, *11*, 1–10.
- (17) Malik, M. A.; Hashim, M. A.; Nabi, F.; Al-thabaiti, S. A.; Khan, Z. Anti-corrosion ability of surfactants: a review. *Int. J. Electrochem. Sci.* **2011**, *6*, 1927–1948.
- (18) Mohanty, U. S.; Tripathy, B. C.; Das, S. C.; Singh, P.; Misra, V. N. Effect of sodium lauryl sulfate (SLS) on nickel electrowinning from acidic sulfate solutions. *Hydrometallurgy* **2009**, *100*, 60–64.
- (19) Anbarasi, C. M.; Rajendran, S.; Pandiarajan, M.; Krishnaveni, A. An encounter with corrosion inhibitors. *Eur. Chem. Bull.* **2013**, *2*, 197–207.
- (20) Kuznetsov, Y. I. *Organic Inhibitors of Corrosion of Metals*; Plenum Press: New York, 1996.
- (21) Tianqing, L.; Aihua, Z.; Rong, G. Effect of surfactant and cosurfactant on the protecting corrosion for nickel. *Acta. Phys. Chim. Sin.* **2000**, *16*, 899–905.
- (22) Vezvaie, M.; Noel, J. J.; Tun, Z.; Shoesmith, D. W. Hydrogen absorption into titanium under cathodic polarisation: an in-situ neutron reflectometry and EIS study. *J. Electrochem. Soc.* **2013**, *160*, C414–C422.
- (23) Wiesler, D. G.; Majkrzak, C. F. Growth and dissolution of protective oxide films on titanium: an in-situ neutron reflectivity study. *Mater. Res. Soc. Symp. Proc.* **1995**, *376*, 247–257.
- (24) Barkhudarov, P. M.; Shah, P. B.; Watkins, E. B.; Doshi, D. A.; Brinker, C. J.; Majewski, J. Corrosion inhibition using super-hydrophobic films. *Corros. Sci.* **2008**, *50*, 897–902.
- (25) Campana, M.; Teichert, A.; Clarke, S.; Steitz, R.; Webster, J. R. P.; Zorbakhsh, A. Surfactant adsorption at the metal-oil interface. *Langmuir* **2011**, *27*, 6085–6090.
- (26) Wood, M. H.; Welbourn, R. J. L.; Charlton, T.; Zorbakhsh, A.; Casford, M. T.; Clarke, S. M. Hexadecylamine adsorption at the iron oxide-oil interface. *Langmuir* **2013**, *29*, 13735–13742.
- (27) Penfold, J.; Thomas, R. K.; Lu, J. R.; Staples, E.; Tucker, I.; Thompson, L. The study of surfactant adsorption by specular neutron reflection. *Phys. B* **1994**, *198*, 110–115.
- (28) Lu, J. R.; Thomas, R. K.; Penfold, J. Surfactant layers at the air/water interface: structure and composition. *Adv. Colloid Interface Sci.* **2000**, *84*, 143–304.
- (29) Penning, F. M.; Moubis, J. H. A. Cathode sputtering in a magnetic field. *Proc. Kon. Ned. Akad. Wetensch.* **1940**, *43*, 41–56.
- (30) Björck, M.; Andersson, G. GenX: an extensible X-ray reflectivity refinement program utilising differential evolution. *J. Appl. Crystallogr.* **2007**, *40*, 1174–1178.
- (31) Parratt, L. Surface studies of solids by total reflection of X-rays. *Phys. Rev.* **1954**, *95*, 359–369.
- (32) Grosvenor, A. P.; Biesinger, M. C.; Smart, R. S. C.; McIntyre, N. S. New interpretations of XPS spectra of nickel metal and oxides. *Surf. Sci.* **2006**, *600*, 1771–1779.
- (33) Drouet, C.; Laberty, C.; Fierro, J. L.; Alphonse, P.; Rousset, A. X-ray photoelectron spectroscopic study of non-stoichiometric nickel and nickel-copper spinel manganites. *Int. J. Inorg. Mater.* **2000**, *2*, 419–426.

- (34) Kim, K. S.; Winograd, N. X-ray photoelectron spectroscopic studies of nickel-oxygen surfaces using oxygen and argon ion-bombardment. *Surf. Sci.* **1974**, *43*, 625–643.
- (35) Rao, S. R. *Surface Chemistry of Froth Flotation*; Kluwer Academic/Plenum Publishers: New York, 2004.
- (36) *Froth Flotation: A Century of Innovation*; Fuerstenau, M. C., Jameson, G., Yoon, R.-H., Eds.; Society for Mining, Metallurgy and Exploration: Littleton, CO, 2007.
- (37) Moriwaki, H.; Yoshikawa, Y. Oxide films on iron and nickel ultrafine particles studied with zero point of charge measurements. *Langmuir* **1990**, *6*, 847–850.
- (38) Smith, L. A.; Hammond, R. B.; Roberts, K. J.; Machin, D.; Mcleod, G. Determination of the crystal structure of anhydrous sodium dodecyl sulfate using a combination of synchrotron radiation powder diffraction and molecular modelling techniques. *J. Mol. Struct.* **2000**, *554*, 173–182.
- (39) Lu, J. R.; Purcell, I. P.; Lee, E. M.; Simister, E. A.; Thomas, R. K.; Rennie, A. R.; Penfold, J. The composition and structure of sodium dodecyl sulfate - dodecanol mixtures adsorbed at the air-water interface: a neutron reflection study. *J. Colloid Interface Sci.* **1995**, *174*, 441–455.
- (40) Feng, S.; Bummer, P. M. Competition of hydrophobic steroids with sodium dodecyl sulfate, dodecyltrimethylammonium bromide, or dodecyl β -D-maltoside for the dodecane/water interface. *Langmuir* **2012**, *28*, 16927–16932.
- (41) Li, N.; Thomas, R. K.; Rennie, A. R. Effect of pH, surface charge and counter-ions on the adsorption of sodium dodecyl sulfate to the sapphire/solution interface. *J. Colloid Interface Sci.* **2012**, *378*, 152–158.
- (42) Wang, X.; Lee, S. Y.; Miller, K.; Stocker, I.; Clarke, S.; Casford, M.; Gutfreund, P.; Skoda, M. W. A. Cation bridging studied by specular neutron reflection. *Langmuir* **2013**, *29*, 5520–5527.
- (43) Aquino, L. I. A. J. A.; Tunega, D.; Schaumann, G. E.; Haberhauer, G.; Gerzabek, M. H.; Lischka, H. The functionality of cation bridges for binding polar groups in soil aggregates. *Int. J. Quantum Chem.* **2011**, *111*, 1531–1542.
- (44) Burgers, J. *Metal Ions in Solution*; Ellis Horwood: Chichester, 1978.
- (45) Somasundaran, P.; Lee, L. T. Polymer-surfactant interactions in flotation of quartz. *Sep. Sci. Technol.* **1981**, *16*, 1475–1490.
- (46) Ma, H.; Chen, S.; Yin, B.; Zhao, S.; Liu, X. Impedance spectroscopic study of corrosion inhibition of copper by surfactants in the acidic solutions. *Corros. Sci.* **2003**, *45*, 867–882.
- (47) Ma, H.; Chen, S.; Zhao, S.; Liu, X.; Li, D. A study of corrosion behaviour of copper in acidic solutions containing cetyltrimethylammonium bromide. *J. Electrochem. Soc.* **2001**, *148*, B482–B488.
- (48) Rudnik, E.; Burzyńska, L.; Dolasiński, Ł.; Misiak, M. Electrodeposition of nickel/SiC composites in the presence of cetyltrimethylammonium bromide. *Appl. Surf. Sci.* **2010**, *256*, 7414–7420.
- (49) Schmitt, G.; Bedbur, K. Investigations on structural and electronic effects in acid inhibitors by AC impedance. *Werkst. Korros.* **1985**, *278*, 273–278.
- (50) Aramaki, K.; Hagiwara, M.; Nishihara, H. Impedance study on inhibition and stimulation of iron corrosion in acid solution by various inorganic anions and tetra-alkylammonium cation. *J. Electrochem. Soc.* **1988**, *135*, 1364–1369.
- (51) Frignani, A.; Zucchi, F.; Monticelli, C. Inhibition of iron corrosion in different acid media by n-decyl-pyridinium derivatives. *Br. Corros. J.* **1983**, *18*, 19–24.
- (52) Jinyun, Z.; Xu, Z.; Dihua, W. The synergistic effect of quaternary ammonium cations on the corrosion inhibition of Fe by inorganic cations. *J. Nat. Sci.* **1996**, *1*, 239–243.
- (53) Hackerman, N.; Snavelly, E. S. J.; Payne, J. S. J. Effects of anions on corrosion inhibition by organic compounds. *J. Electrochem. Soc.* **1966**, *113*, 677–681.
- (54) Franchi, M.; Ferris, J. P.; Gallori, E. Cations as mediators of the adsorption of nucleic acids on clay surfaces in prebiotic environments. *Org. Life. Evol. Biosph.* **2003**, *33*, 1–16.
- (55) Liu, G. Q.; Zhu, Z. Y.; Ke, W.; Han, E. H.; Zeng, C. L. Corrosion behaviour of stainless steels and nickel-based alloys in acetic acid solutions containing bromide ions. *Corrosion* **2001**, *57*, 730–738.
- (56) Shein, A. B.; Ivanova, O. S.; Minkh, R. N. The effect of anions on the anodic dissolution of nickel silicide in sulfate electrolytes. *Prot. Met.* **2008**, *44*, 32–44.
- (57) Bergstrom, P.-A.; Lindgren, J. An IR study of the hydration of ClO_4^- , NO_3^- , I^- , Br^- , Cl^- and SO_4^- anions in aqueous solution. *J. Phys. Chem.* **1991**, *95*, 8575–8580.
- (58) Marcus, Y. Ionic radii in aqueous solutions. *Chem. Rev.* **1988**, *88*, 1475–1498.
- (59) Morales-Gil, P.; Walczak, M. S.; Cottis, R. A.; Romero, J. M.; Lindsay, R. Corrosion inhibitor binding in an acidic medium: Interaction of 2-mercaptobenzimidazole with carbon-steel in hydrochloric acid. *Corros. Sci.* **2014**, *85*, 109–114.
- (60) Molchan, I. S.; Thompson, G. E.; Lindsay, R.; Skeldon, P.; Likodimos, V.; Romanos, G. E.; Falaras, P.; Adamova, G.; Iliev, B.; Schubert, T. J. S. Corrosion behaviour of mild steel in 1-alkyl-3-methylimidazolium tricyanomethanide ionic liquids for CO_2 capture applications. *RSC Adv.* **2014**, *4*, 5300–5311.